Clim Dyn
DOI 10.1007/s00382-017-3643-8

Predecessor rain events over China's low-latitude highlands associated with Bay of Bengal tropical cyclones

Junpeng Yuan[1] · Di Zhao[1] · Ruowen Yang[1,2] · Hongfei Yang[3]

Received: 18 May 2016 / Accepted: 16 March 2017

Abstract A predecessor rain event (PRE) is defined as organized heavy rainfall that occurs far ahead of tropical cyclone (TC), yet directly associated with the deep tropical moisture originating from the TC vicinity. The PREs occurring over China's low-latitude highlands (CLLH) in association with Bay of Bengal TCs were investigated from 1981 to 2012. Results indicate that about 19% of Bay of Bengal TCs produces PRE. The PREs frequently occur when TCs are active in the northern Bay of Bengal with northeastward paths. The PREs are more likely to appear in the pre-monsoon and post-monsoon seasons, with peaks in May and October, respectively. The median lifetime of the PREs was approximately two days. The distances between PREs and parent TCs are ranged from 745 to 1849 km, with a median distance of 1118 km. Composite results of PREs suggested that deep moisture is advected from the TC vicinity to the remote CLLH region, which is situated beneath the equatorward entrance of the upper-level East Asia subtropical jet (EASJ). The lower-level southwesterly flow, which is associated with a strong pressure gradient between the western Pacific subtropical high and a trough in Bay of Bengal, steers TCs conveying abundant moisture from the Bay of Bengal to the CLLH region. The enhancement of the ascent and frontogenesis within the equatorward entrance region of the EASJ is favorable for occurrence of PREs in CLLH. TCs may also have a dynamical role in occurrence of PREs by intensifying the upper-level EASJ.

1 Introduction

Low-latitude highlands are defined as areas where the average altitude exceeds 1500 m above sea level at latitudes below 30°N (e.g., Tao et al. 2013; Cao et al. 2014). In China, low-latitude highlands are situated in the southwest, which includes Yunnan, southern Sichuan, and western Guizhou and Guangxi provinces (Qin et al. 1997). The topography and landforms of China's low-latitude highlands (CLLH) are complex and fragmentary. In this area, the highest altitude is in the northwest and over 6000 m above sea level, nevertheless the lowest altitude in the southeast is below 100 m (Fig. 1). CLLH region lies on the southeast of the Qinghai-Tibetan Plateau and is close to the tropical Bay of Bengal (BOB) and South China Sea. The CLLH is jointly influenced by tropical and mid-latitude weather systems (Cao et al. 2014; Li and Zhou 2015), among which, tropical cyclones (TCs) originating from the BOB are declared to be a severe threat when approaching CLLH (Duan et al. 2009). For example, the BOB tropical cyclone Akash on 15–17 May 2007 caused three days of heavy precipitation over CLLH, with the maximum accumulated rainfall exceeding 270 mm. The extremely severe tropical cyclone Nargis, caused 70,000 deaths in Myanmar on 3 May 2008 (Webster 2008), also produced heavy rainfall and led to the initiation of the rainy season in CLLH (Xiao et al. 2011). Moreover, owing to the complex and fragmentary landscape in CLLH, heavy rainfall over the region often leads to secondary disasters, such as landslides

✉ Junpeng Yuan
jpyuan@ynu.edu.cn

[1] Department of Atmospheric Sciences, Yunnan University, Kunming 650091, China

[2] Key Laboratory of Meteorological Disaster of Ministry of Education, Nanjing University of Information Science and Technology, Nanjing, China

[3] Meteorological Bureau of Honghe County in Yunnan province, Honghe, China

Published online: 29 May 2017

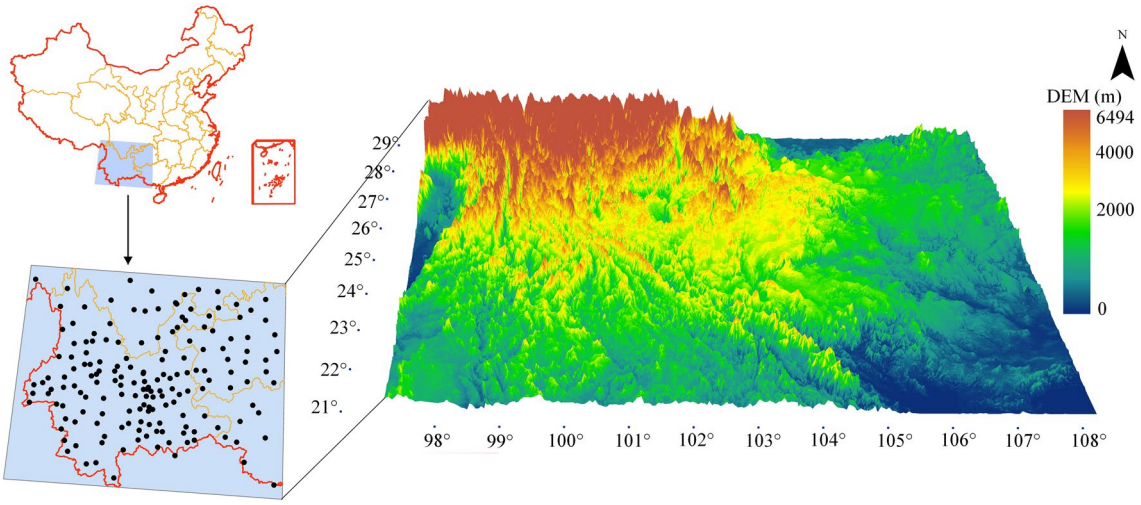

Fig. 1 Location and terrain of China's low latitude highlands (CLLH). *Black dots* indicate rainfall gauge stations. The topography of CLLH is presented using digital elevation model (DEM) in *shading color*

and debris flows, causing serious economic losses and great social impacts (Tao et al. 2013).

In general, BOB TCs are often separated by long distances from CLLH. Even when a TC lands on the northeastern coast of the BOB, the minimum distance between it and CLLH is about 600 km. When approaching CLLH, TCs are usually weakened by the blocking effect of mountains, such as the Himalayas, the Naga Mountains, and the Hengduan Mountains in CLLH. In contrast to TCs generated in the western North Pacific and South China Sea, which can make landfall over China and have direct effects, the influence of BOB TCs on CLLH is comparatively indirect. Few BOB TC land directly in the CLLH region. However, the remnants of BOB TC can remain active for a few days after TC extinction and in consequence generate strong rainfall in the CLLH region (Wang et al. 2009b), especially when TC remnants are encountered and interact with other weather systems, Such as subtropical high, South Asian high, Indian-Burma trough, subtropical jet and quasi-stationary fronts (e.g., Duan et al. 2009; Xiao et al. 2011; Xu et al. 2014). Occasionally, the influence of BOB TC also can spread downstream to South China and even to the middle and lower branches of the Yangtze-Huaihe River Basin (Lü et al. 2013).

Numerous studies also suggested that the BOB TCs may produce remote heavy rainfall in CLLH before TC's landfall. Satellite cloud images indicate that broad zonal cloudy belts extend from BOB TC vicinity to the heavy rainfall regions in CLLH (e.g., Duan and Duan 2015; Xiao et al. 2011). The BOB TCs may provide plentiful warm and moist air to the CLLH region, and cause remote heavy rainfall therein. This remote effect of TC is different with the direct rainfall that produced by TC or TC remnants.

Previous studies had already pointed out that TCs can produce heavy rainfall at large distances from the TC vortex, especially when TCs interact with other mid-latitude systems (Pierce 1939; Bosart and Carr 1978). This remote effect of TCs can be referred to as remote, indirect, or distant precipitation (Bosart and Carr 1978; Chen 2007; Wang et al. 2009a). The remote precipitation is also an important constituent of TC-related precipitation, besides the well-known rain shields surrounding the TC vortex (Wang et al. 2009a; Chen et al. 2010). Cote (2007) examined remote precipitation cases related to Atlantic Ocean TCs, and suggested the term 'predecessor rain event' (PRE) to describe the organized heavy rainfall that occurs far ahead of a TC, yet is intimately connected to it.

By indentifying PREs based on TC–PRE separation distance and the deep moisture advection directly associated with TCs, PREs occurring over the United States in association with Atlantic TCs have been extensively investigated from case study and synoptic climatology perspectives (Cote 2007; Galarneau et al. 2010; Schumacher et al. 2011; Bosart et al. 2012; Schumacher and Galarneau 2012; Moore et al. 2013). An important aspect for PRE occurrence is the poleward advection of deep tropical moisture originating from the TC vicinity into PRE regions. The PREs typically occur over low-level baroclinic zones, beneath the equatorward entrance of an upper-level jet, when deep warm moist air originating from the TC vicinity is transported poleward and forced to ascend (Cote 2007; Galarneau et al. 2010; Moore et al. 2013). Moore et al. (2013) summarized that PREs differ from ordinary heavy rainfall by the possible dynamical and thermodynamic contributions of the TC, such as

associated water vapor transport and interactions with the low-level baroclinic zone and upper-level jet.

Wang et al. (2009a) examined the contribution of the western North Pacific TC Songda to distant heavy rainfall in Japan. Byun and Lee (2012) indicated that TCs generated in the western North Pacific can produce approximately half of the total precipitation in Korean Peninsula. Recently, Cong et al. (2014) showed that 27 provinces of China are influenced by remote heavy precipitation associated with western North Pacific TCs, including some regions of CLLH, which are also influenced by TCs from the BOB. Compared with numerous studies on the precipitation of TCs generated in the western North Pacific and the Atlantic Ocean, there are relatively fewer studies of the remote effect of BOB TCs on precipitation in CLLH. Furthermore, relevant previous studies mostly used case studies to show qualitative results of the circulation environments which are favorable for BOB TCs producing heavy rainfall in CLLH. The quantitative examinations of the remote effect of BOB TCs from a climatological perspective are lacking.

This study focused on the remote heavy rainfall effect of BOB TCs on CLLH. Predecessor rain events (PREs) were employed to quantitatively represent the remote effect of BOB TCs on CLLH. The aim of this study was to (1) determine the climatology of PREs occurring in CLLH associated with BOB TCs; and (2) examine the typical environments and development mechanisms for PREs over CLLH.

The remainder of this paper is organized as follows. The datasets and methods are described in Sect. 2. In Sect. 3, the climatology and statistical analysis of the relationship between BOB TCs and PREs over CLLH are presented. Composite analysis of the typical synoptic environments and possible factors for the development of PREs is shown in Sects. 4 and 5, respectively. Finally, a summary and discussion is provided in Sect. 6.

2 Data and methodology

2.1 Datasets

The following datasets were used in this study for the period 1981–2012.

1. Daily precipitation data observed at 170 stations over CLLH. The dataset was provided by the China Meteorological Administration (CMA). The gauge station locations over CLLH are shown in Fig. 1.
2. The best-track dataset for TCs from the Joint Typhoon Warning Centre (JTWC). This dataset contains TC locations and intensities over the BOB at 6 h intervals (Chu et al. 2002).
3. Daily reanalysis datasets (including geopotential height, specific humidity, zonal winds, meridional winds, vertical winds, and sea-level pressure) from the National Centers for Environmental Prediction-National Center for Atmospheric Research (NCEP-NCAR) Reanalysis Project with a horizontal resolution of 2.5°×2.5° and a vertical resolution of 17 levels (Kalnay et al. 1996; Kistler et al. 2001).
4. The six-hourly ERA-Interim atmospheric reanalysis produced by the European Center for Medium Range Weather Forecasts. The dataset is at T255 spectral (~80 km) resolution but that it was interpolated to a regular 0.75° horizontal grid, and the vertical resolution is 32 levels (Dee et al. 2011).

In addition, the daily gridded Asian precipitation highly resolved observational data (APHRO) with a horizontal resolution of 0.5°×0.5° from 1981 to 1997 (Yatagai et al. 2009) and the satellite based precipitation analyses from the Tropical Rainfall Measuring Mission (TRMM) 3B42 version 6 with a horizontal resolution of 0.25°×0.25° from 1998 to 2012 (Kummerow et al. 1998) were also used.

2.2 PRE identification

Following Cote (2007) and Galarneau et al. (2010), PREs were identified by determining whether deep tropical moisture is advected from the TC vicinity to CLLH heavy rainfall regions. PREs were selected based on the following criteria:

- A coherent area of rainfall over CLLH persisting for at least 24 h.
- An average rainfall rate of ≥25 mm per 24 h for at least three gauge stations in CLLH over the entire lifetime of the PRE.
- The coherent rainfall region in CLLH is clearly separate from the area of rain directly tied to a TC vortex.
- Deep tropical moisture originally associated with the TC must be advected away from the TC vicinity into the CLLH coherent rainfall region.

Cote (2007) and Galarneau et al. (2010) defined PREs based on radar imagery. However, there are no complete radar data available for CLLH before 2006. In this study, PREs were selected based on daily observation precipitation data from the CMA. The selection criteria were (1) high-impact PREs in CLLH with a rainfall rate ≥25 mm per 24 h for at least three stations and (2) more than 20 stations with 5 mm or greater daily rainfall around the candidate PRE area, excluding isolated rainfall events. The criterion of 25 mm per 24 h is based on the heavy rain advisory of the CMA.

The search for TC-related PREs was carried out by manually determining whether the deep tropical moisture input originated directly from TCs to a coherent area of rainfall over CLLH within the period of TC occurrence. In the study period, sequential heavy rainfall associated with the same TC was treated as one PRE. By examining 28 PREs east of the Rocky Mountains in the United States during 1995 to 2008, Galarneau et al. (2010) found that most TCs were generally weakening at the time of PRE occurrence, and about 25% of PREs' parent TCs were at tropical depression strength. Therefore, in this paper, TCs with tropical depression strength or greater were examined, including tropical depressions, cyclonic storms, severe cyclonic storms, extremely severe cyclonic storms, super cyclonic storms. Examination began when a TC reached at least tropical depression strength.

An important aspect of PREs is that deep tropical moisture originally associated with the TC must be advected poleward into the PRE region, typically manifested as total-column precipitable water (TPW) values greater than 40–50 mm (Cote 2007; Galarneau et al. 2010; Schumacher et al. 2011; Moore et al. 2013). Following Galarneau et al. (2010) and Moore et al. (2013), maps of TPW and the synoptic-scale flow analysis generated from the NCEP-NCAR reanalysis dataset, were manually examined for each prospective case to assess whether the deep tropical moisture originated directly from the TC vicinity. Noting that the elevation of CLLH is relatively high and the average climatological TPW over CLLH is less than 25 mm, in this study TPW values are chosen as greater than 35 mm, which is approximately 1 standard deviation higher than climatological value over CLLH.

The APHRO dataset from 1981 to 1997 and the TRMM data from 1998 to 2012 were used to examine whether the remote areas of rain associated with PREs were indeed clearly separated from the areas of rain directly tied to a TC. If the area of rain directly tied to a TC, which is represented as an area surrounded with 5 mm rainfall isoline in TC vicinity, is separated from the candidate PRE rainfall area, the case is selected as PRE case.

The Hybrid Single-Particle Lagrangian Integrated Trajectory (HYSPLIT) model (version 4.9) was also used for each prospective PRE in verifying whether the air parcels and associated water vapor originated from TC vicinity (The model is available online at: http://ready.arl.noaa.gov/HYSPLIT.php). The backward air parcel trajectories were calculated by using HYSPLIT model and NCEP\NCAR reanalysis dataset. In HYSPLIT model, it assumes that a particle passively follows the winds, with its trajectory being the integration of its position vector in space and time (Draxler and Hess 1998). Hourly values of meteorological variables including the pressure, height, temperature, and relative humidity etc. are provided along each trajectory. The backward air parcel trajectories were calculated as follows: over the rainfall area in CLLH, air parcels were released from locations which on a 2.5 by 2.5° grid area, respectively. The air parcels were released at 6h intervals within the period of candidate PRE occurrence. The backward tracking was beginning at 1500 m height above surface. TC vicinity is defined as an area which surrounded a TC vortex with TPW value greater than 40 mm. Trajectories of which the backward tracking provenance was located in the TC vicinity were determined as originated from the TC. If there exits trajectory sourced from the TC vicinity, the case was determined as PRE.

2.3 Composite analysis

Composite analysis methods have proven effective for investigating the favorable atmospheric environments of TC-related heavy rainfall (Galarneau et al. 2010; Byun and Lee 2012; Moore et al. 2013). In this study, geographical composite methods were utilized to examine the atmospheric environments of TC-related PREs. In Sect. 4, to explore the similarities and differences in the synoptic-scale atmospheric structure between heavy rainfall and no heavy rainfall events for given locations of TCs, the geographical composite analyses were generated using both the NCEP-NCAR reanalysis dataset and ERA interim dataset for PREs and no heavy rainfall events (NHREs), respectively. The results obtained by the two datasets are very consistent, and we just show the results calculated by using the NCEP-NCAR reanalysis dataset in Sect. 4.

In Sect. 5, to illustrate the time evolution and more detailed spatial features of the TC-related PRE circulation fields, the composites were computed at PRE initiation (T − 0), 24 h before PRE initiation (T − 24), and 24 h after PRE initiation (T + 24) using the six-hourly higher resolution ERA-Interim datasets. All the composite anomalies were compared with the weighted monthly long-term climatology for 1981–2012. The two-sided Student's *t*-test, which gives the probability that the means for two groups are statistically different at the 95% confidence level, was used for significance tests.

The two-dimensional horizontal frontogenesis function, which was first defined by Petterssen (1936) and formulated by Ninomiya (1984), was computed based on the ERA-Interim dataset to investigate the role of frontogenesis in focusing vertical motion and associated precipitation in PREs. The evaluation for frontogenesis is computed as the change rate of the magnitude of the horizontal equivalent potential temperature (θ_{se}) gradient.

The curve clustering method was also used for extract the typical tracks of the parent TCs in PRE and NHRE groups. The curve clustering method is based on the polynomial regression mixture model, which employs

conditional mixture density estimation to uncover cluster memberships among a set of curves (Gaffney 2004). The conditional densities are defined as functions of longitudinal and latitudinal positions of the cyclones conditioned on the observation time. A Matlab toolbox with the clustering algorithms is available online at http://www.datalab.uci.edu/resources/CCT.

3 Climatology of PREs during 1981–2012

A total of 21 PREs that occurred over CLLH during 1981–2012 were identified as being associated with 21 BOB TCs. Approximately 19% of all BOB TCs can produce PRE over CLLH. As shown in Fig. 2, BOB TC genesis mainly occurs in two peak seasons. One is documented as the pre-monsoon season of April–May, and the other is the post-monsoon season of September–November. PRE parent TCs also exhibit two peak seasons, but with different details. Over the whole BOB basin, TCs more frequently occur in the post-monsoon season with a peak in October, appear relatively uniform throughout the pre-monsoon season, and PRE parent TCs tend to occur evenly in pre- and post-monsoon seasons (Fig. 2). PREs preferentially occurred with TCs that formed in May and October, with 33 and 29% of all PREs occupying those months, respectively, compared with 18 and 31% of all BOB TCs. However, nearly 68% of the TCs that did not produce a heavy rainfall event over CLLH occurred in the post-monsoon season, particularly in October and November. Hence, once generated in the BOB, the probability of a TC producing a PRE over CLLH in the pre-monsoon season is larger than in the post-monsoon season.

Approximately 19% of PREs were associated with strong TCs that reach at least category 3 intensity, meanwhile 57 and 24% occur with TCs that reach tropical storm (TS) and category 1–2 intensity, respectively (Fig. 3). The distribution for TC intensity at the time of PRE initiation presents general weaker than the maximum TC intensity. Examination of individual cases shows that nearly 57% of PREs (12 in total of 21) initiate before the parent TC reaching the maximum strength. Approximately 81% of all PRE parent TCs are at or weaker than TS strength at the time of PRE initiation. These results suggested that the BOB TCs which are even at very weak intensity may also produce PREs over CLLH.

TCs originated in the BOB mainly produce heavy rainfall in the southwest of CLLH (Fig. 4a). The average precipitation of PREs decreases from the southwest to northeast, which is consistent with the elevation gradient in CLLH (Fig. 1). Figure 5 shows the frequency of heavy rainfall days associated with PREs over CLLH and the related parent BOB TC locations at the time of PRE occurrence in each grid box. During the period of 1981–2012, PREs produce 1.2 days heavy rainfall per year, which contributes about 15% of the total heavy rainfall days in CLLH (~8 days, Yang et al. 2014). Heavy rainfall frequently occurs in the southwest of CLLH when TCs are passing over the northern BOB or making landfall in Myanmar, Bangladesh, and northeastern India, especially when TCs are east of 85°E and north of 15°N. The frequency of PRE-related heavy rainfall days shows a banded distribution, decreasing from the southwest to northeast (Fig. 5b). In addition, there is also a zonal high-frequency region in the east downstream of CLLH. Case study analysis indicated that the TC PRE-related rainfall belts can occasionally extend from CLLH to farther eastward downstream, even to the middle-lower branches of the Yangtze-Huaihe River Basin (figures not shown). These results are consistent with Lü et al. (2013), who found that BOB TCs not only affect CLLH,

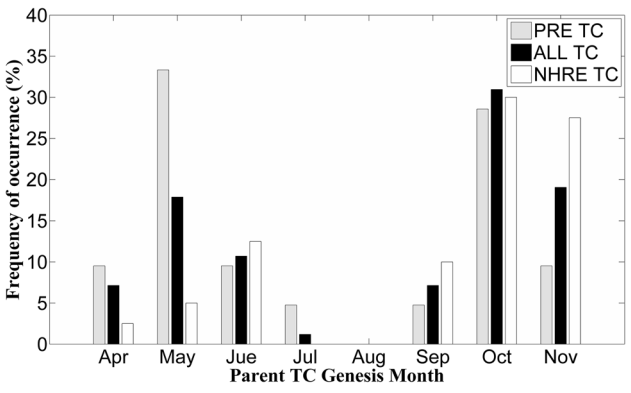

Fig. 2 Monthly frequency distribution of all TCs in the BOB (*black bars*), TCs that produced PREs over CLLH (*gray bars*), and TCs with no heavy rainfall (NHRE, clear *bars*) over CLLH during 1981–2012

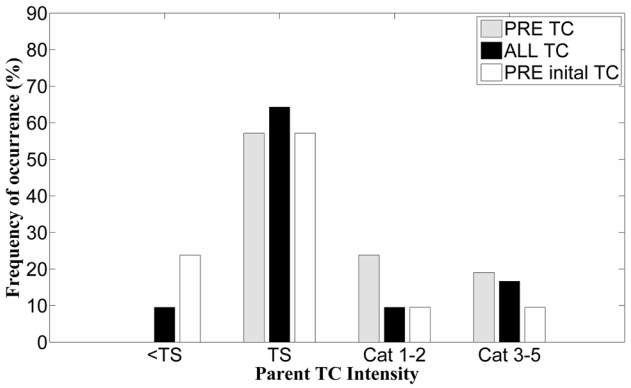

Fig. 3 The frequency distribution of maximum TC intensity of all TCs in the BOB (*black bars*) and TCs that produced PREs over CLLH (*gray bars*) during 1981–2012 according to Saffir-Simpson scale category. Additionally, the frequency distribution of parent TC intensity at the time of PRE initiation is shown in *clear bars*

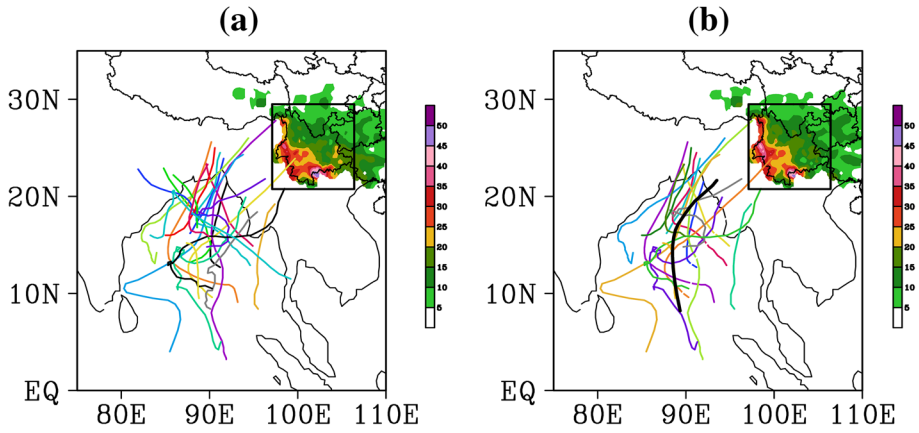

Fig. 4 **a** Tracks of TCs that produced PREs over CLLH and associated process-averaged precipitation distribution (unit: mm) during 1981–2012. **b** Same as (**a**), but for northeastward track TCs. The *black bold line* is the average track for the PRE-related northeast-path TCs

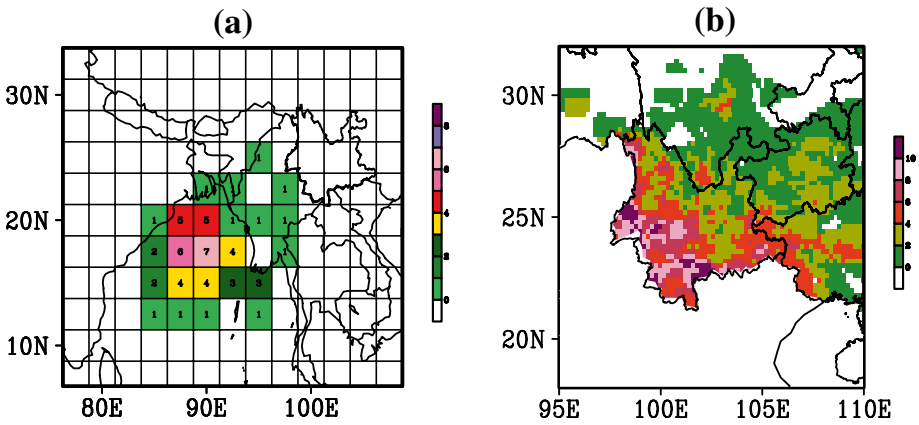

Fig. 5 **a** Geographical distribution of TC location frequency in each 2.5×2.5 *grid box* at the time of PRE occurrence over CLLH. **b** Frequency of heavy rainfall days associated with BOB TC-related PREs over CLLH in each 0.2×0.2 *grid box*

but also impact the downstream regions of CLLH along the westerly zone.

Cluster analysis indicates that the typical paths of TCs that produced PREs in CLLH are northeastward and northwestward tracks. The dominant track is northeastward path, and exceeding 80% of total TCs (17 in total of 21) follow northeastward tracks. The precipitation produced by 17 northeast path TCs are averaged in Fig. 4b. The distributions and magnitudes of precipitation are very similar with Fig. 4a, with slightly lager rainfall in western frontier of CLLH. Further statistical analysis shows that 41% of all northeastward path TCs in the BOB produced PREs over CLLH during 1981–2012.

The box-and-whisker plots of PRE lifetime, heavy rainfall areal extent, maximum PRE rainfall, and distances between the TCs and associated initial PRE centers are shown in Fig. 6. The PRE center is defined as the location of the maximum heavy rainfall of initial PRE in CLLH. The median PRE lifetime is 2 days, with the shortest (longest) lifetime being one day (3 days). The areal extent of heavy rainfall related to TC PLREs is represented as the percentage of CLLH in experiencing heavy rainfall ($\geq$25 mm d^{-1}). The median areal extent of heavy rainfall occupies approximately 11% area of CLLH, ranging from 6 to 23% for the 25th and 75th percentiles, respectively (Fig. 6b). Sometimes, BOB TCs can produce exceptionally widespread PREs. For example, No. 200602 TC was associated with heavy rainfall in 44% of the CLLH. The maxima of daily rainfall range from 40 to 123 mm, with a median maximum rainfall of 73 mm. The 25th and 75th percentiles maxima daily rainfall for PREs are 60 and 100 mm, respectively (Fig. 6c). The distances between the PREs and parent TCs vary widely from 745 to 1849 km, with a median distance of 1118 km.

4 Typical synoptic-scale environments favorable for PREs

To explore the favorable environments for PRE occurrence, this study compared the synoptic atmospheric environments of PREs with those of NHREs for given locations of TCs. Because the majority of high-impact PREs occur in CLLH when parent TCs track north of 15°N (Fig. 5a), the cases in which the parent TC in the BOB tracked north of 15°N in its lifetime but did not generate heavy rainfall

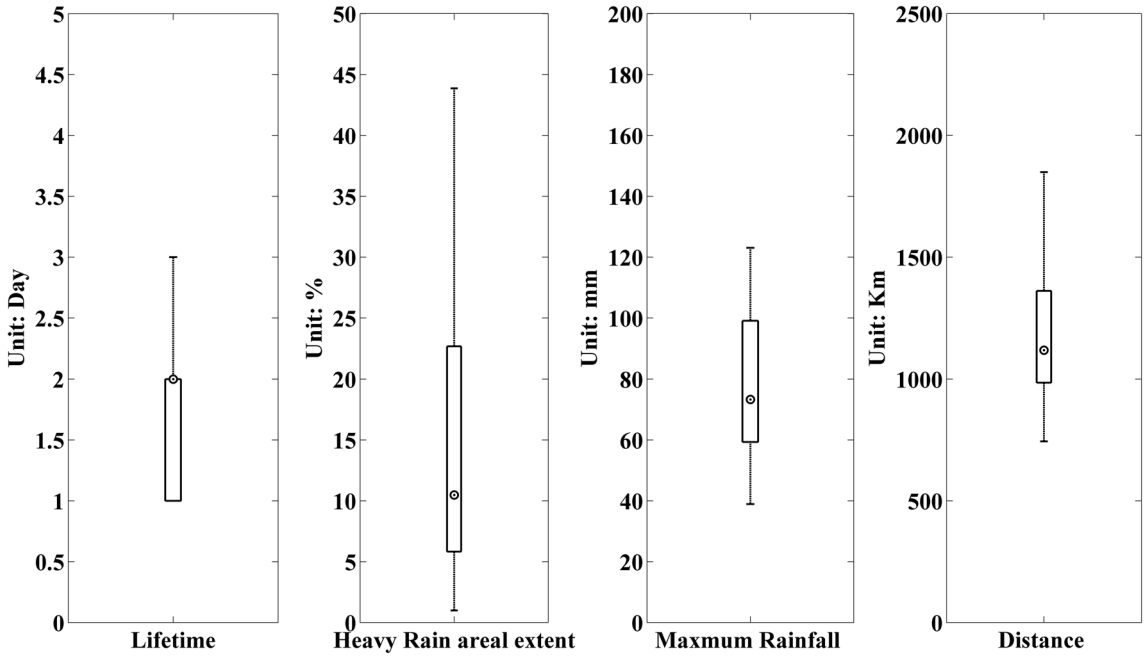

Fig. 6 Box-and-whisker diagrams of **a** PRE lifetime (days), **b** PRE areal extent of heavy rainfall (the percentage of CLLH in experiencing heavy rainfall (≥25 mm d^{-1})), **c** maximum PRE rainfall (mm), and **d** distance (km) between the TC and PRE region at the time of PRE occurrence. The lower (*upper*) bound of the box marks the 25th (75th) percentile, and the *solid circle* indicates the median value. The *whiskers mark* the maximum and minimum values. The + symbol indicates outliers

in CLLH were selected as the NHRE group. For PREs, the parent TCs are predominantly follow northeastward tracks. To determine the key atmospheric environments which are favorable for PREs that produced by TCs in tracking northeastward paths, the composite of 17 PREs that related to northeastward path parent TCs (refer as PRE_NE group) are also investigated.

Geographical composites of the atmospheric environments for 21 PRE, 40 NHRE and 17 PRE_NE cases were generated using the NCEP-NCAR daily reanalysis datasets. For the PRE and PRE_NE cases, the composite analyses were computed using the whole lifetime of the TC-related PRE occurrence. Approximately 71% of PREs (15 of 21) occurred on the same day, 24 h before, or 48 h before TC landfall. Therefore, the NHREs for the day of TC landfall, 24 h before TC landfall, and 48 h before TC landfall were used to generate the NHRE group composite analysis. If the TC did not made landfall, the composite analysis of the day of TC extinction was used.

For the PRE cases, the average TC location is in the northern BOB when TCs were producing PREs over CLLH (Fig. 7a). As the reflection of TC circulations, significant anomalous low geopotential height appears from the BOB to south of the Qinghai-Tibet Plateau. Note that the anomalous low geopotential height in northern BOB may also relates to the south branch westerly shortwave trough (referred to as the Indian-Burma trough, Li and Zhou 2016). Approximately 38% of PREs (8 of 21 PREs) were occurring with appearance of the Indian-Burma trough in northern BOB. The western Pacific subtropical high expands from the western North Pacific to the South China Sea and Indo-China Peninsula, with a single subtropical high cell centered in the South China Sea. In the mid-latitudes, the geopotential field presents a pattern of one trough in the East Asia and one ridge in 90°E. The East Asia longwave trough locates near the coast of the eastern China. Anomalous low geopotential height expands from the BOB and eastern China to north of CLLH region, respectively. Meanwhile, anomalous high geopotential height appears in south of CLLH region (Fig. 7a). Associated with these anomalous distributions of geopotential height field, significant anomalous southwesterly flow is present in the eastern flank of the TCs and west of the South China Sea subtropical high (Fig. 8a). The strong southwesterly flow is favorable for steering TCs and associated water vapor from the BOB to the PRE regions in CLLH (Fig. 9a). Strong ascent expands from southern Thailand to the CLLH (Fig. 9a).

In the NHRE composites, significant anomalous low geopotential height is centered in western coast of BOB. Distinct positive geopotential height anomalies present from the Indo-China Peninsula to CLLH and even to the north of China. This forms a meridional high-pressure barrier (Fig. 7b), which is unfavorable for moisture transport from the BOB to CLLH. For NHRE cases, the parent TCs

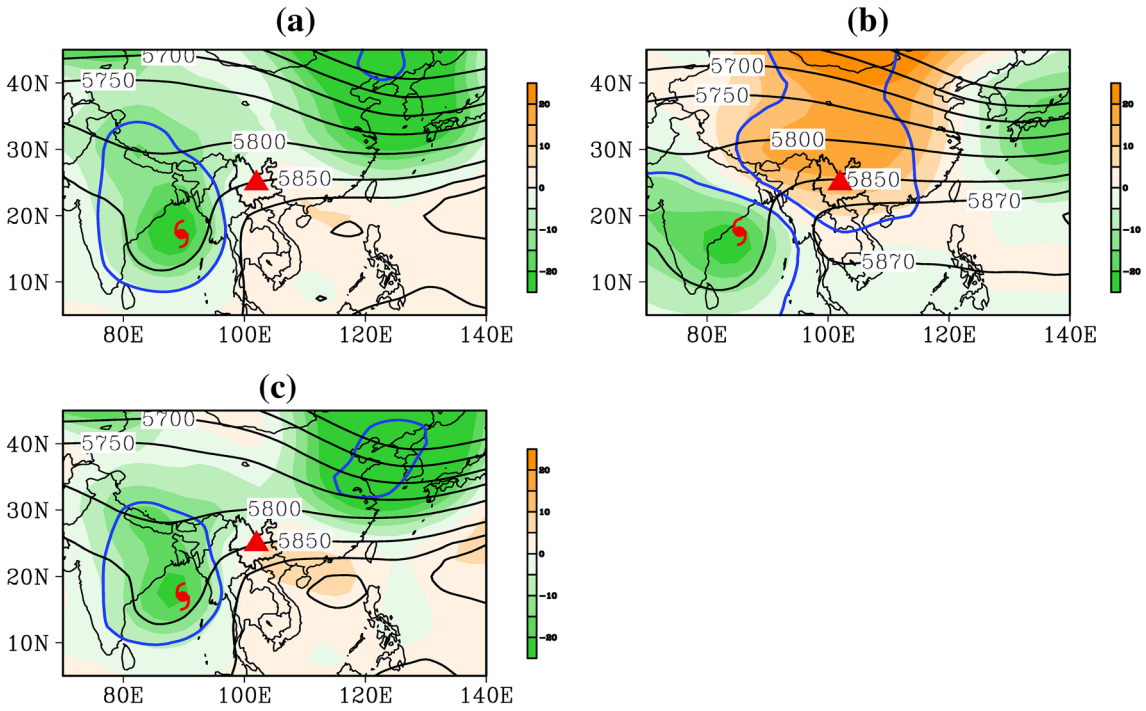

Fig. 7 Composite maps of geopotential height (*solid line*, unit: m) and anomalous geopotential height (*shaded*, unit: m) at 500 hPa for **a** 21 PRE cases, **b** 40 NHRE cases, and **c** 17 PRE_NE cases. Anomalous geopotential heights that are statistically different from the weighted monthly long-term (1981–2012) climatology at 95% significance level are indicated by *blue solid contours*. The composite TC locations are indicated by *tropical storm symbols*. The CLLH location center is indicated by *triangle mark*

are located in the northwestern BOB. Significant southerly wind and strong water vapor fluxes are also mainly exhibited in the northern BOB (Figs. 8b, 9b). Accordingly, strong water vapor convergence (Fig. 9b) and ascent are confined to the surrounding areas of the northern BOB (Fig. 8b).

At 200 hPa, a well-defined upper-level westerly jet, which is located over the East Asia between 30 and 40°N and documented as the East Asia subtropical jet (EASJ, Huang et al. 2014), is present in both PRE and NHRE groups. However, the detailed upper level circulation patterns and jet locations are different between the PRE and NHRE categories. For PREs, the upper-level EASJ is positioned at 30°N, and the CLLH is situated beneath the equatorward entrance of the EASJ (Fig. 10a). This configuration is favorable for forcing an anomalous ascending branch of circulation over the CLLH (Fig. 11a). Conversely in the NHRE composites, the EASJ is located farther westward to 85°E, and the favorable environments are not present (Figs. 10b, 11b).The PRE_NE composites are very similar to those of PRE. Meanwhile, compared with the PREs, the PRE_NE group presents stronger upper-level EASJ and associated stronger ascent over CLLH.

The significance test of the differences between PRE and NHRE composites are shown in Fig. 12a. Distinct negative differences of 500 hPa geopotential height appear from northern BOB and CLLH regions to the middle latitudes. The 700 hPa meridional wind presents that significant positive differences appear in east coast of BOB and CLLH regions. These indicate that the low-level southerly flow extended from the BOB to CLLH region in PREs is significantly stronger than that in NHREs. The strong southerly flow can steers TC conveying abundant water vapor from the BOB to CLLH in PRE cases (Figs. 8a, 9a). As a result, the differences of TPW show significant positive values in eastern BOB coast and CLLH region (Fig. 12a). The differences of 200 hPa zonal wind present significant negative values in west of the CLLH between 30–40°N, suggesting that the locations of the upper-level EASJ and associated ascent branch of circulation are also significantly different in PREs and NHREs. The differences between the PRE_NE and NHRE groups (Fig. 12b) feature similar patterns as in Fig. 12a.

Furthermore, in PRE and PRE_NE cases, the wind in the eastern flank of TCs veers from southwesterly at 700h Pa (Fig. 8a) to westerly at 200 hPa (Fig. 10a). Anomalous warm temperature expands from the TC vicinity to CLLH in the troposphere with centered near 300 hPa (Fig. 11a, c). The warm air ascends from the TC vicinity and moves northeastward to CLLH. Deep warm-air advection anomalies appear in the troposphere. The centers of anomalous warm-air advection are located at 200 hPa, which generally is the maximum level of the TC outflow. TCs likely interact

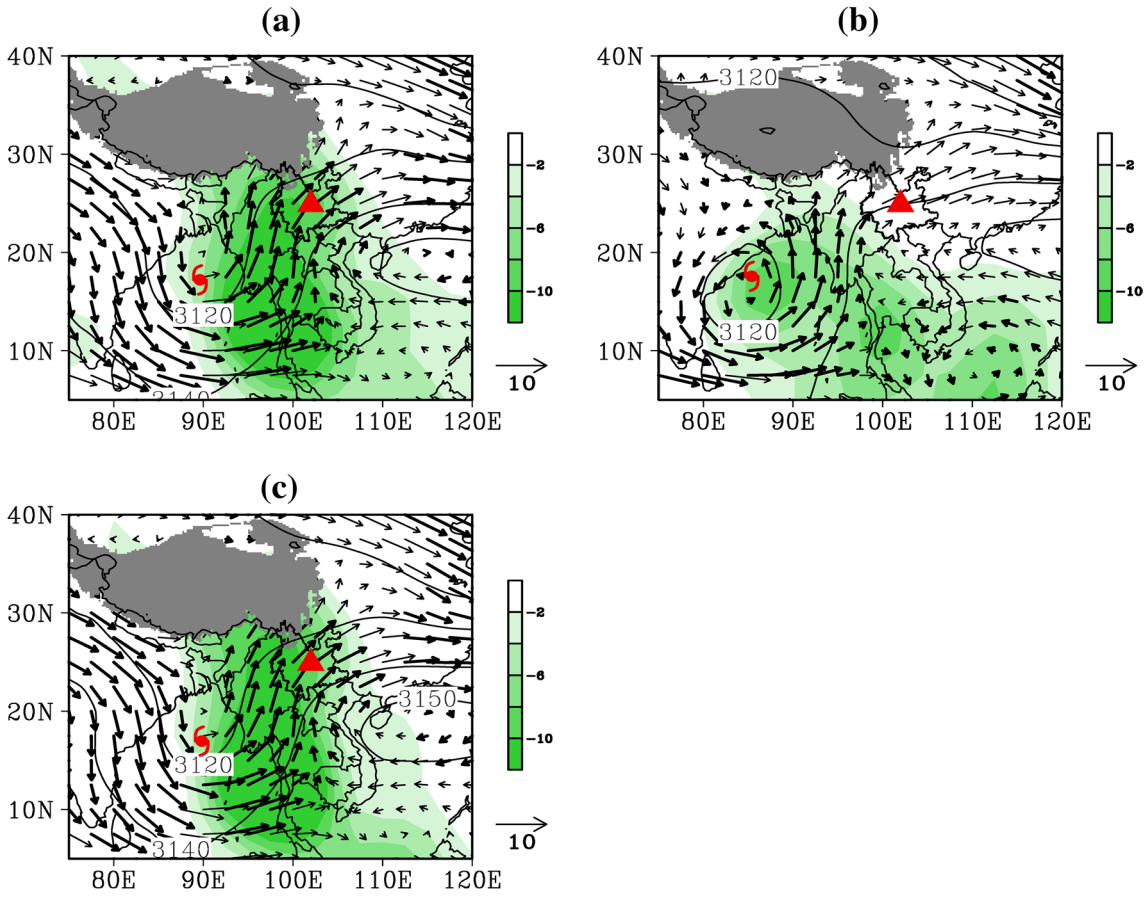

Fig. 8 Composite maps of wind field (vectors, unit: m s^{-1}), geopotential height (*solid line*, unit: m) at 700 hPa, and vertical velocity at 500 hPa (*shaded*, unit: 10^{-2} pa s^{-1}) for **a** 21 PRE cases, **b** 40 NHRE cases, and **c** 17 PRE_NE cases. *Bold black* wind vectors indicate 700 hPa meridional wind anomalies that are statistically different from the weighted monthly long-term (1981–2012) climatology at 95% significance level. The composite TC locations are indicated by *tropical storm symbols*. The CLLH location center is indicated by *triangle mark*

with the upper-level jet through this warm-air advection. Numerous studies presented that the diabatically driven outflow from the TC can injects into the southern flank of the upper-level jet, and produces increases of the potential vorticity gradient and wind speeds along the jet streak (e.g., Galarneau et al. 2010; Bosart et al. 2012; Moore et al. 2013). The warm air advection from TC vicinity may strengthen the upper-level EASJ and the associated ascent over CLLH. The detailed processes will be discussed in next section.

5 Mechanisms of PRE development

Cluster analysis indicated that over 80% of TCs follow northeastward tracks when producing PREs in CLLH (17 in total of 21). To illustrate the time evolution and detailed spatial features of PRE development, 17 PREs cases which the parent TCs track as northeast-path are utilized to generate the composite analysis. The composites are computed at PRE initiation (T − 0), 24 h before PRE initiation (T − 24), and 24 h after PRE initiation (T + 24).

5.1 Moisture configurations

At T − 24, the western North Pacific subtropical high expands westward to the South China Sea and a deep trough is situated in the BOB (Fig. 13a). A strong pressure gradient between the subtropical high and the BOB trough is favorable for strengthening the southwesterly flow in the eastern coast of the BOB, and therefore steering TCs conveying abundant tropical moisture poleward (Fig. 13b). Correspondingly, a broad plume of high TPW with a maximum greater than 60 mm can be found in the eastern flank of TCs (Fig. 13a). Accompanying with TC's approaching to the coast at T − 0, higher TPW caused by the stronger southwesterly flow and the convergency of water vapor flux extends northeastward from the TC vicinity to CLLH

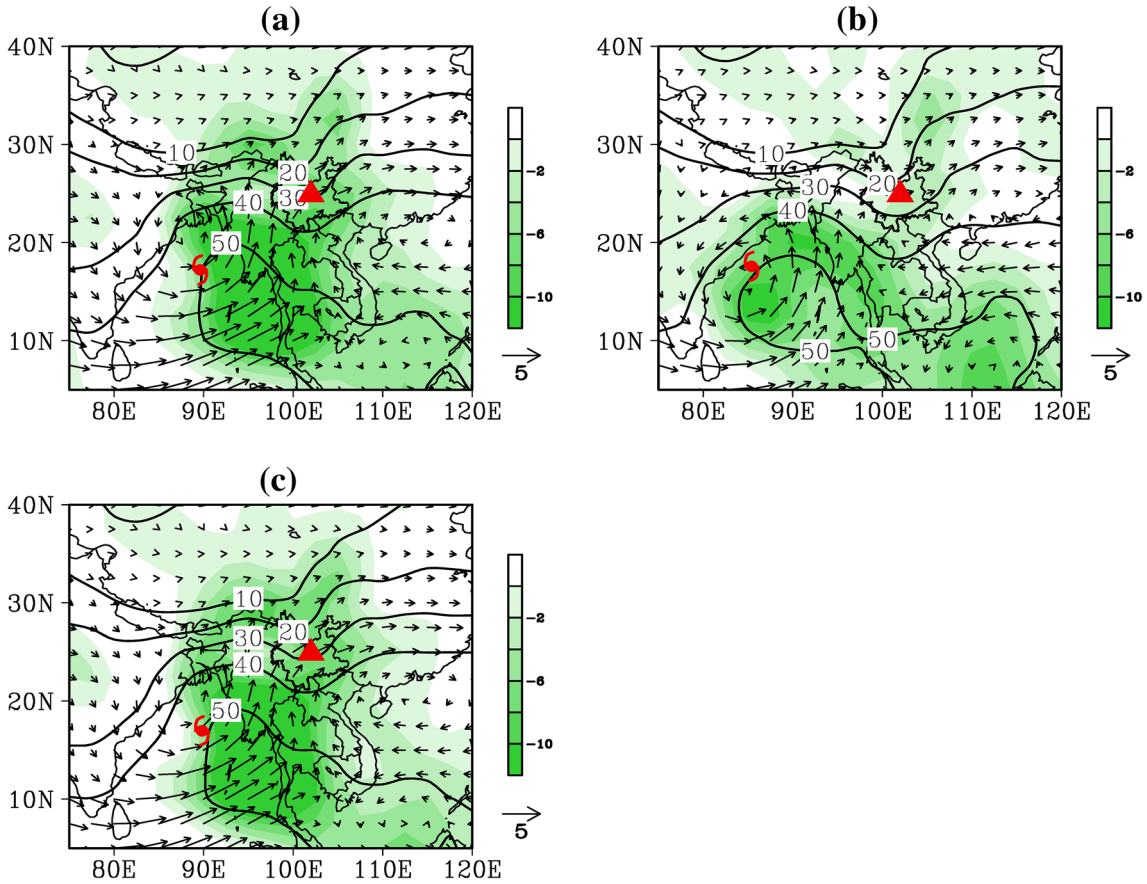

Fig. 9 Composite total-column precipitable water (contours, unit: mm), column-integrated water vapor flux (vectors, unit: 10^3 g m^{-1} s^{-1}), and divergence of column-integrated water vapor flux (*shaded*, unit: g m^{-2} s^{-1}) for **a** 21 PRE cases, **b** 40 NHRE cases, and **c** 17 PRE_NE cases. The composite TC locations are indicated by *tropical storm symbols*. The CLLH location center is indicated by *triangle mark*

(Fig. 13c, d). The composite TPW over CLLH is statistically different from the weighted monthly long-term climatology according to the two-sided Student's *t* test (figure not shown).

The HYSPLIT model was used for each PRE to tracking the sources of the air parcels and associated water vapor. As described in Sect. 2, air parcels were released from the PRE regions at 6h intervals within the period of PRE occurrence. The backward tracking was beginning at the height of 1500 m above surface. Trajectories of which the backward tracking provenance was located in the TC vicinity were determined as originated from the TC. The average trajectory of the air parcels originated from the TC vicinity to CLLH for 17 PRE cases is shown in Fig. 13c (the bold blue line), and the associated air parcels' pressure and relative humidity backward time series are shown in Fig. 14. Results of the HYSPLIT model indicate that the median time of the air parcels transported from the TC vicinity to CLLH PRE region is about 72 h. Time series of the air parcel pressure indicate that the air parcels ascended as they approaching the PRE regions in CLLH. The relative humidity time series show that the air parcels remained moist with the median values approximately 80%, suggesting that abundant water vapor was transported from the TC vicinity to CLLH along the average trajectory.

The average air parcel and associated water vapor transport trajectory is matched well with the southwesterly flow in the low level. The southwesterly flow is important for conveying moist air from the TC vicinity to the PRE regions. According to the average trajectory shown in Fig. 13c, the starting and ending points of the average trajectory (A point, 89°E, 15°N; B point, 101°E, 24°N), and farther east downstream of CLLH (C point, 120°E, 24°N) are linked by red solid lines (Fig. 13d). Detailed composite vertical cross-sections for moisture along the ABC line segment are shown in Fig. 15. At T − 24, an area of enhanced moisture extends from the TC vicinity, and moves northeastward to CLLH along the mountain windward slope, which agrees with the moist air ascent from TC vicinity to the CLLH shown in Fig. 14. At T − 0, strong southwesterly

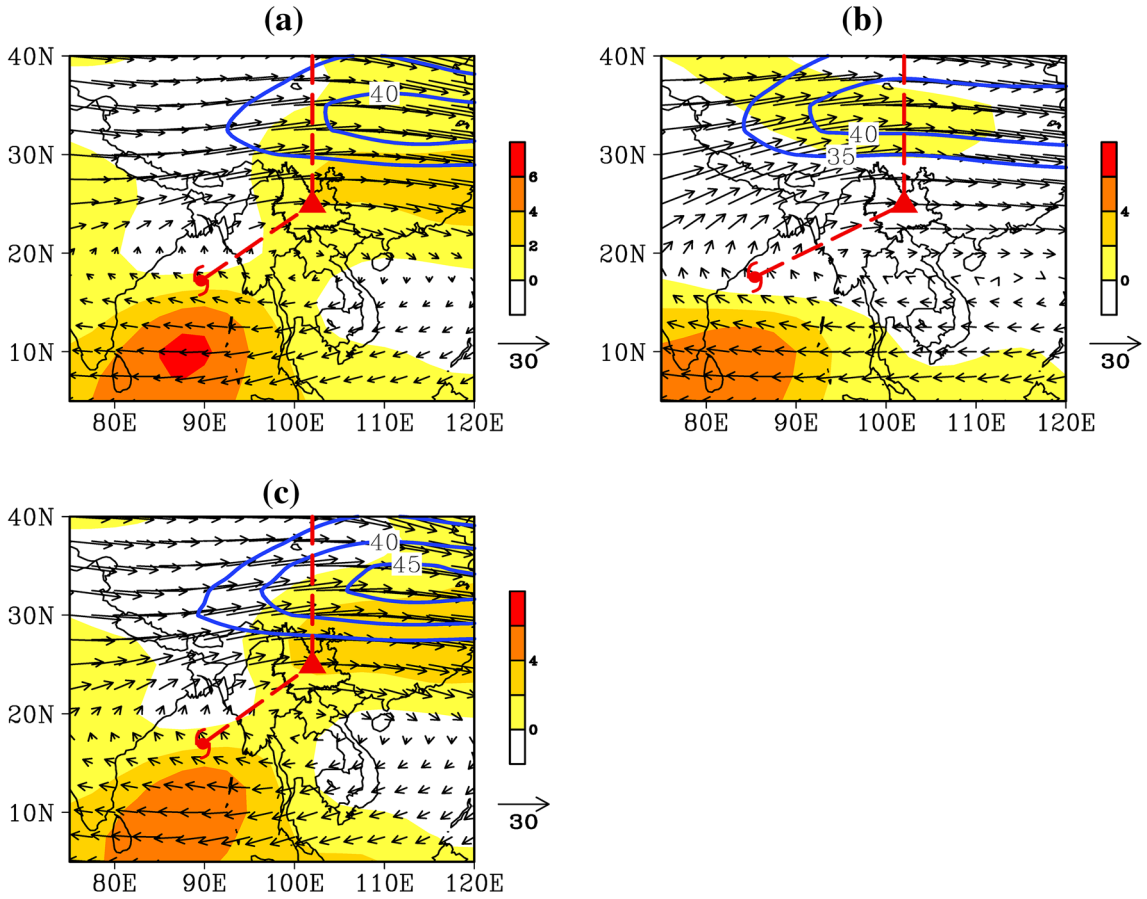

Fig. 10 Composite wind field (vectors, unit: $m\,s^{-1}$), and zonal wind anomaly (shaded, unit: $m\,s^{-1}$) at 200 hPa for **a** 21 PRE cases, **b** 40 NHRE cases, and **c** 17 PRE_NE cases. Zonal wind speeds greater than 35 $m\,s^{-1}$ are indicated by blue solid contours. The composite TC locations are indicated by *tropical storm symbols*. The CLLH location center is indicated by *triangle mark*

flow and water vapor flux appear in the eastern flank of TCs (Fig. 13c, d). Along the ABC line segment, the vertical section of the composite water vapor flux presents that strong moist air ascends from TC vicinity and is transported to the CLLH. Positive humidity anomalies can be found from the ground to top of the troposphere with a maximum lying at 850 hPa (Fig. 15b). The center of water vapor flux moves northeastward to CLLH, indicating that deep moisture is transported into CLLH. At T + 24, slightly weakened water vapor flux presents in the eastern flank of TCs (Fig. 13f). Meanwhile, the meridional plume of high TPW is still maintained in the eastern flank of the TC (Fig. 13e).

During the period of PRE' evolution from T − 24 to T + 24, tropical and subtropical environments, in which the TCs are embedded, hold steady (Fig. 13a, c, d). The western North Pacific subtropical high is dominates over the South China Sea, and a steady trough is maintained in the BOB. The peripheral southerly airflow of the subtropical high can merge with the southwesterly wind in front of the BOB low trough, and therefore steer TCs transporting tropical moisture poleward (Fig. 13). Thus, deep moisture is conveyed northeastward and provides abundant water vapor for the development of PRE in CLLH. Accompanying the approach of TC, positive humidity anomalies appear consistently from the bottom to top of the troposphere over CLLH, and strong water vapor transport related to TCs can expands to 400 hPa (Fig. 15). This is evidently different from the climatological feature that water vapor is mainly concentrated in the lower troposphere below the 700 hPa layer over CLLH (Zheng et al. 2013). The anomalous increase of the moisture in midtropospheric may lead to thickening of the saturated moist layer, which is favorable for heavy rainfall occurrence over CLLH.

5.2 Lifting and frontogenesis

At T − 24, upward motion dominates in the northern BOB and the periphery of the western North Pacific subtropical high. Strong ascent appears in the east flank of TCs and extends northeastward to CLLH (Fig. 16a). This coincides quite well with low-level frontogenesis. Intense frontogenesis mainly appears in the northwestern Indo-China

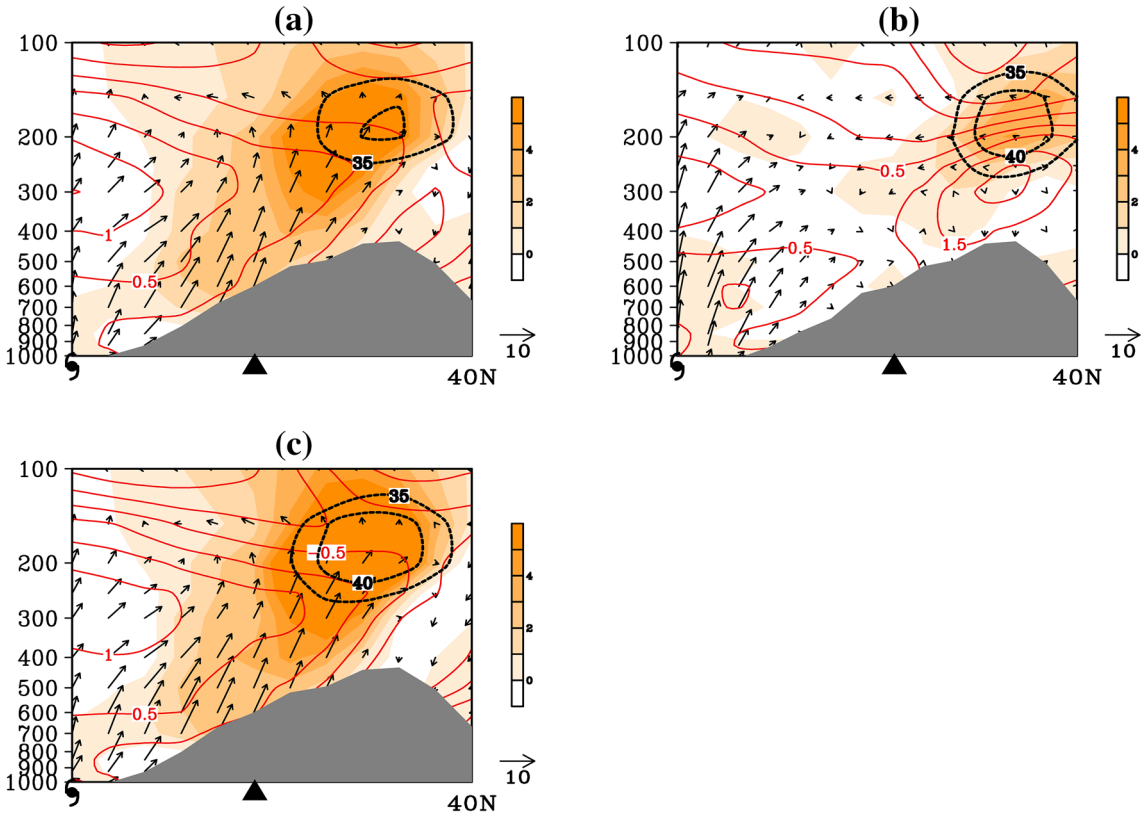

Fig. 11 Composite vertical cross-sections for **a** 21 PRE cases, **b** 40 NHRE cases, and **c** 17 PRE_NE cases of temperature advection anomaly (*shaded*, Unit: 10^{-5} K s^{-1}), temperature anomaly (*red contours*, Unit: K), wind flow anomaly (vector, the *horizontal* flow in m s^{-1} and the *vertical* flow is in 10^{-2} Pa s^{-1} and zonal wind speed (every 5 m s^{-1} from 35 m s^{-1}, *black lines*) along the red dotted lines in Fig. 10. The composite TC locations are indicated by *tropical storm symbols*. The CLLH location center is indicated by *triangle mark*

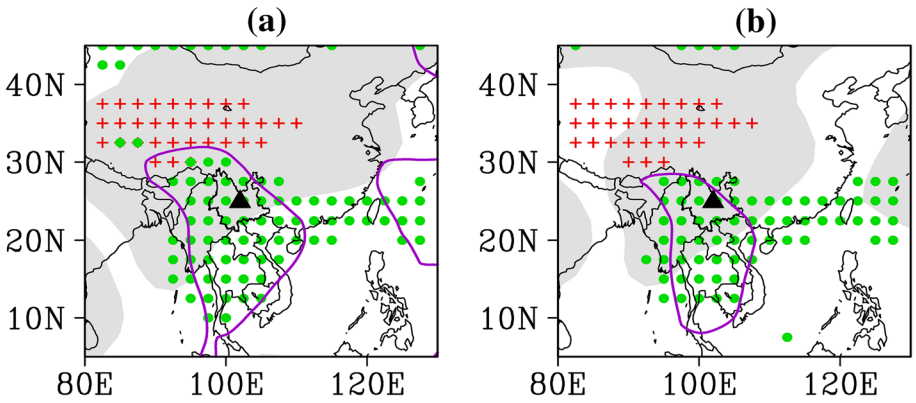

Fig. 12 The significance t-test of the differences between PRE and NHRE cases (**a**), and between PRE_NE and NHRE cases (**b**). *Green dots* (*Red* crosses) denote the positive (negative) differences of TPW (200-hPa zonal wind component) passing the significance test at 95% confidence level. *Gray shaded* (*Purple* contours) denote the negative (positive) differences of 500-hPa geopotential height (700-hPa meridional wind component) passing the significance test at 95% confidence level. The CLLH location center is indicated by *triangle mark*

Peninsula and the west of CLLH, and the south edge of the Qinghai-Tibetan Plateau. Strong southwesterly flow appears in the eastern flank of TC and extends to the northeastern coast of the BOB (Fig. 16b). Note that the topography of CLLH is higher in the northwest and lower in the southeast (Fig. 1). The southwesterly flow impinges upon the mountains almost perpendicularly. The southwesterly winds can cause strong convergence, and may thus force ascent and

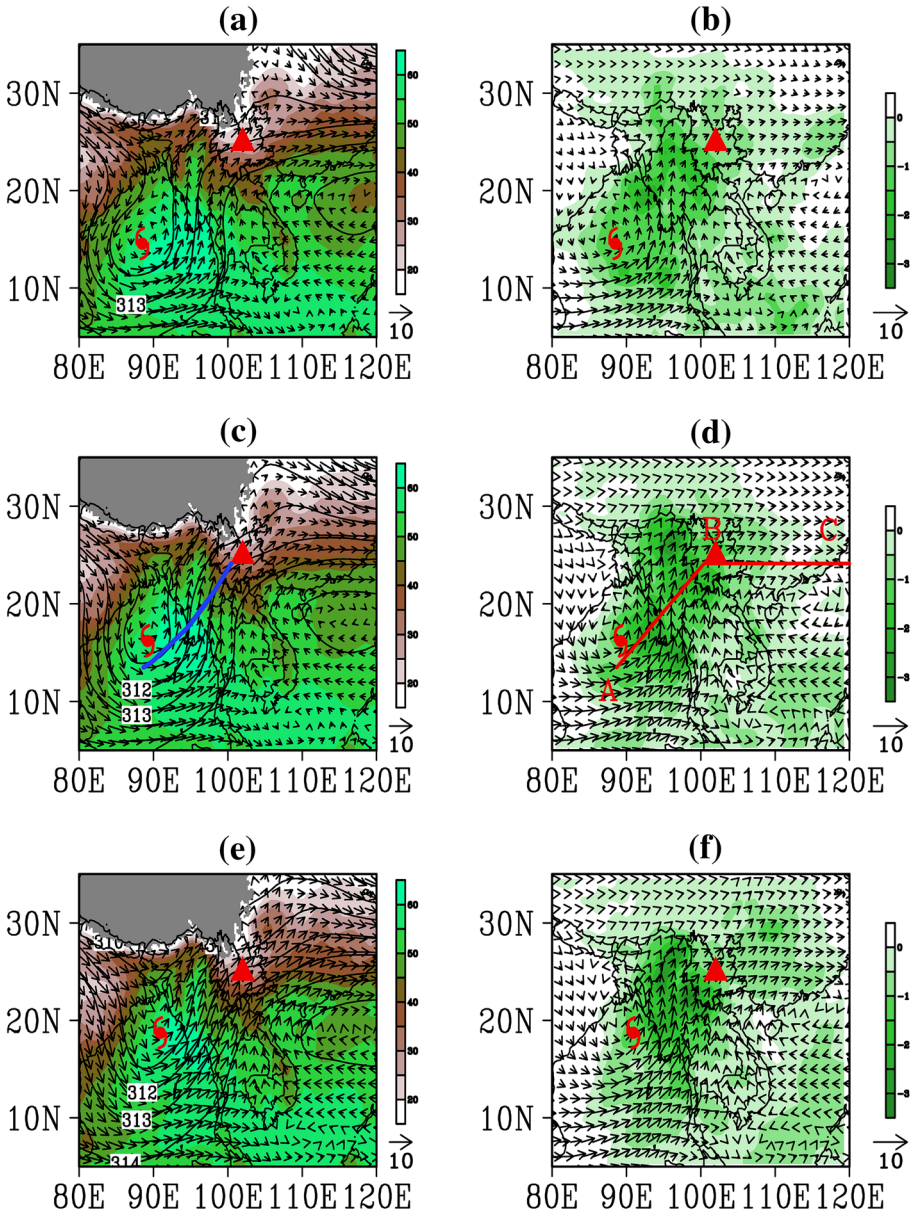

Fig. 13 Composites for 17 PRE_NE cases of 700 hPa geopotential height (*contour*, unit: gpdm), 700 hPa wind (vector, unit: m s^{-1}), and total-column precipitable water (*shaded*, unit: mm) in left panels, and column-integrated water vapor flux (vector, unit: 10^3 g m^{-1} s^{-1}) and divergence of column-integrated water vapor flux (*shaded*, unit: g m^{-2} s^{-1}) in right panels at T − 24 (**a, b**), T − 0 (**c, d**), and T + 24 (**e, f**). The associated composite PRE-related parent TC locations are labeled with TC symbols. The CLLH location center is indicated by *triangle mark*. The *blue line* denotes the average trajectory of the air parcels and associated water vapor originated from the TC vicinity to the CLLH for 17 PRE cases, which is extracted according to the backward trajectory cases of HYSPLIT model. The starting point (A point, 89°E, 15°N) and ending point (B point, 101°E, 24°N) of the average trajectory, and farther east downstream of CLLH (C point, 120°E, 24°N) are linked by a *red solid line*

frontogenesis on the windward slope side. Strong ascent can be found from the ground to 300 hPa on the windward slope side over CLLH (Fig. 17b). The area of high relative humidity is extended above 700 hPa (Fig. 17a). In addition, the northerly downdraft appears in north of 30°N as shown in Fig. 17b. The cold flow intrudes to the south along the east edge of the Qinghai-Tibetan Plateau and is juxtaposed with the southwesterly warm and moist air, resulting in frontogenesis.

At T − 0, strengthened southwesterly wind appears from the east flank of TC to the CLLH (Fig. 16d), ascent and frontogenesis are also obviously intensified, especially in the south and west of CLLH (Fig. 16c, d). On the one hand, the strengthened southwesterly flow leads to stronger convergence under orographic forcing in the southwest of CLLH, thus intensifies frontogenesis therein. On the other hand, the strong southwesterly flow conveys more abundant warm and moist air poleward to CLLH. This can increase the thermal gradient and intensify frontogenesis in CLLH (Fig. 17c, d). The analysis of 700 hPa equivalent potential temperature shows a θ_{se} ridge. The PRE occurs on the northeastward flank of the θ_{se} ridge in a region of strong deformation (Figure not shown) and frontogensis at 700 hPa.

Accompanying strengthening of frontogenesis (Fig. 16d) and the upward expansion of the high relative humidity region (Fig. 17c), the equivalent potential temperature field also shows that a narrow belt with dense isolines is uplifted northward over CLLH (Fig. 17c). Acclivous ascending motion can be found consistently from the lower to upper

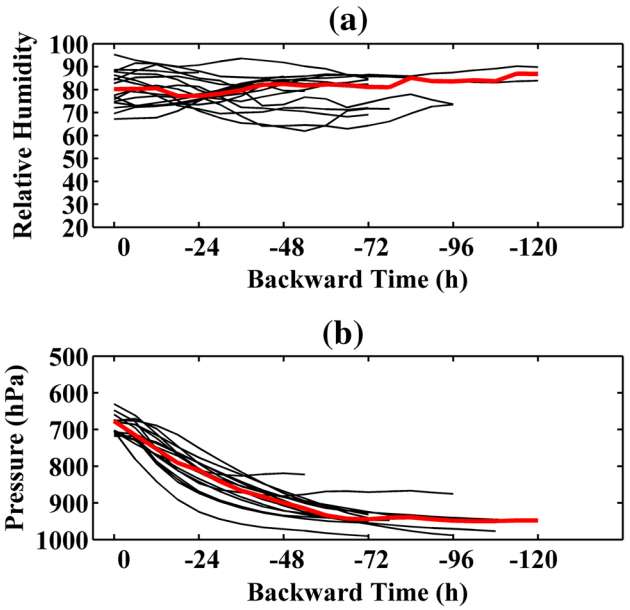

Fig. 14 Backward time series of the median air parcel **a** relative humidity (%) and **b** pressure (hPa) for air parcels originating within the BOB TCs vicinity generated according to the backward trajectory cases of HYSPLIT model. The *red lines* indicate the median values for 17 PRE_NE cases

troposphere over CLLH (Fig. 17d). This is beneficial for transporting abundant moisture upward and weakening atmospheric stability. Associated with TCs' approaching to the coast at T + 24, frontogenesis is slightly weakened (Figs. 16f, 17f).

5.3 EASJ intensification associated with PRE occurrence

It is worthy to note that a narrow upper-level westerly jet, which is described as the EASJ spreading from the eastern Qinghai-Tibetan Plateau to East Asia, is well-defined in the composite PRE-related upper-level circulation in Fig. 10. Between T-24 and T-0h, the EASJ strengthens from 48 to 54 $m s^{-1}$ (Fig. 18), and remains nearly stationary. The intensification of the EASJ is in the 24-h period leading up to PRE initiation. The intensification of the EASJ contributes to the occurrence of PREs, which are located beneath the equatorward jet entrance region. Conversely, the intensification of the EASJ may be also related to TCs and PREs. Heavy precipitation-producing systems, such as TCs and PREs, are often associated with deep ascent and strong latent heat release, and thus may diverged diabatically driven outflow in the upper level. Previous studies indicated that the upper-level diabatically driven outflow can interact with the upper-level jet by impinging on the potential vorticity (PV) gradient along the axis of the jet (Bosart et al. 2012; Moore et al. 2013).

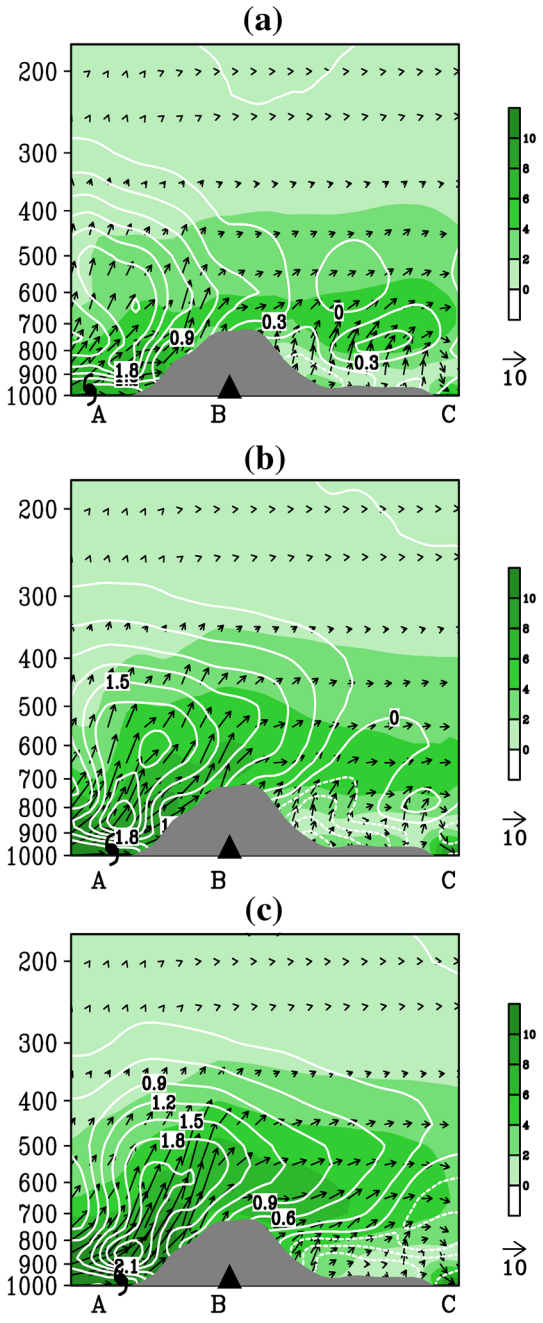

Fig. 15 Composite vertical cross-sections of water vapor flux (*horizontal* direction vector, unit: 10^{-2} m s^{-1}, *vertical* direction unit: 10^{-5} m s^{-1}), magnitude of water vapor flux (*shaded*, unit: 10^{-2} m s^{-1}), and anomalous specific humidity (*contour*, unit: g kg^{-1}) for 17 PRE_NE cases along the ABC line segment shown in Fig. 13d at T − 24 (**a**), T − 0 (**b**), and T + 24 (**c**). The composite TC locations are indicated by *tropical storm symbols*. The CLLH location center is indicated by *triangle mark*

Following Bosart et al. (2012) and Moore et al. (2013), the 250–200 hPa layer average composite analyses from T − 24 to T + 24 were computed to investigate the physical processes that contribute to the EASJ intensification.

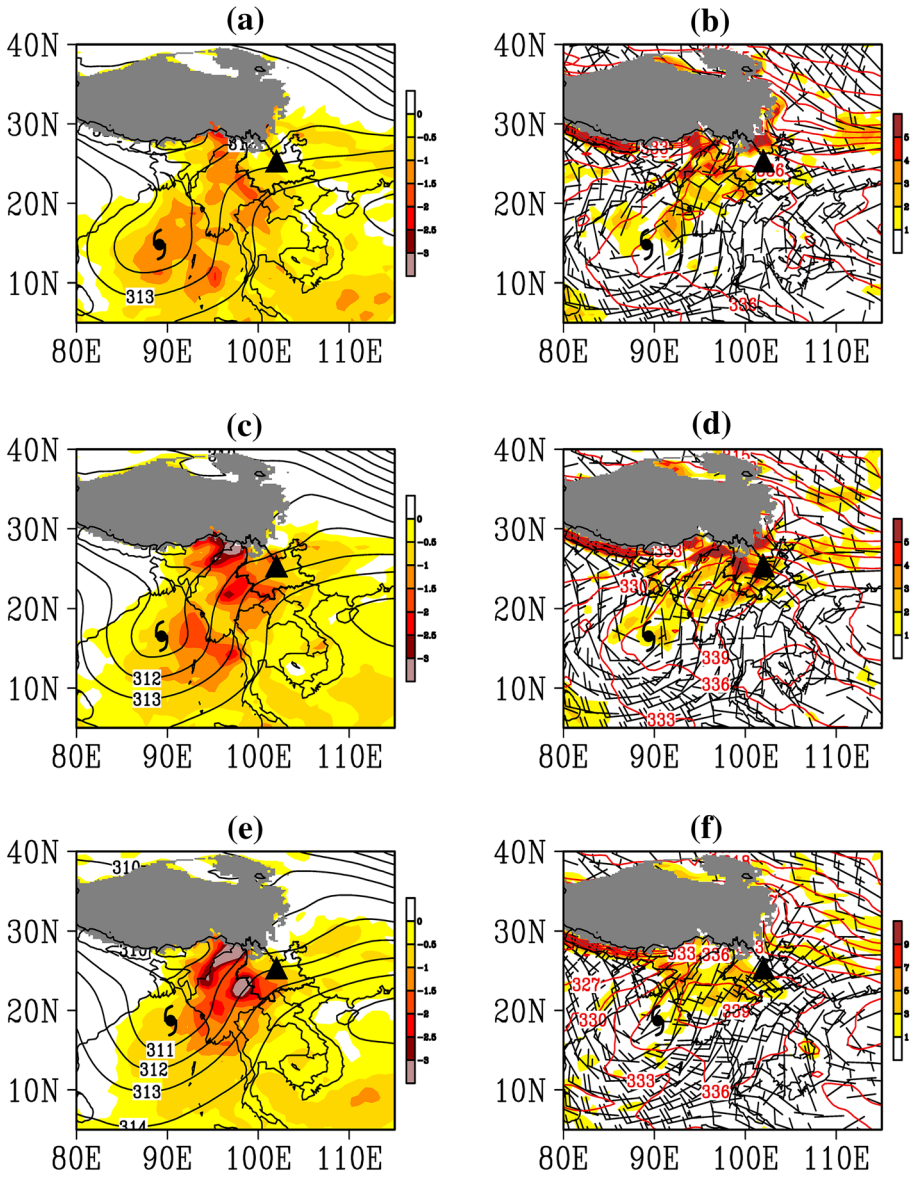

Fig. 16 Same as Fig. 13, but for 700 hPa geopotential height (*contour*, unit: gpdm), and 500 hPa vertical velocity (*shaded*, unit: 10^{-1} pa s^{-1}) in left panels, and 700 hPa wind (barbs, full barb = 5 m s^{-1}), 700 hPa frontogenesis (*shaded*, unit: 10^{10} K m^{-1} s^{-1}), and equivalent potential temperature (*red contour*, unit: K) in *right panels* at T − 24 (**a, b**), T − 0 (**c, d**), and T + 24 (**e, f**)

The winds were decomposed as irrotational and nondivergent component. The anomalous irrotational wind and PV advection by the anomalous irrotational wind in the 250–200 hPa layer were used to examine the dynamical and thermodynamic interactions between the diabatically driven outflow associated with the PRE and/or the TC and the upper-level EASJ.

At T − 24, the EASJ is located in south of the 200-hPa East Asia trough and northeast of CLLH (Fig. 18a). Low-level strong ascent expands from the east flank of TC to the equatorward entrance region of the EASJ (Fig. 18b). Anomalous strong irrotational winds are directed westward and northward from the TC and the ascent region. The irrotational winds linked to low-PV diabatic outflow are directed poleward into the jet entrance region toward larger values of PV, yielding negative PV advection by the irrotational wind therein. From T − 24 to T − 0, the jet entrance region remains approximately stationary above the PRE region. The 200 hPa East Asia trough also maintains located in the downstream of the EASJ and is dominated with high-PV air (Fig. 18a, b). Meanwhile, accompanying with the northeastward movement of TC and initiation of PRE, low-PV air expands northward and eastward. The meridional PV gradient between the areas of high- and low-PV air increases. Strong negative PV advection anomalies linked with strengthened irrotational wind appear in south of the EASJ (Fig. 18d), reinforcing the intensification of the EASJ. Thus, the negative PV advection, which is associated with the diabatically driven outflow of the TC and PRE and concentrated in the EASJ entrance region by the irrotational wind, likely contributes to the maintenance of a large PV gradient and the EASJ intensification. In addition,

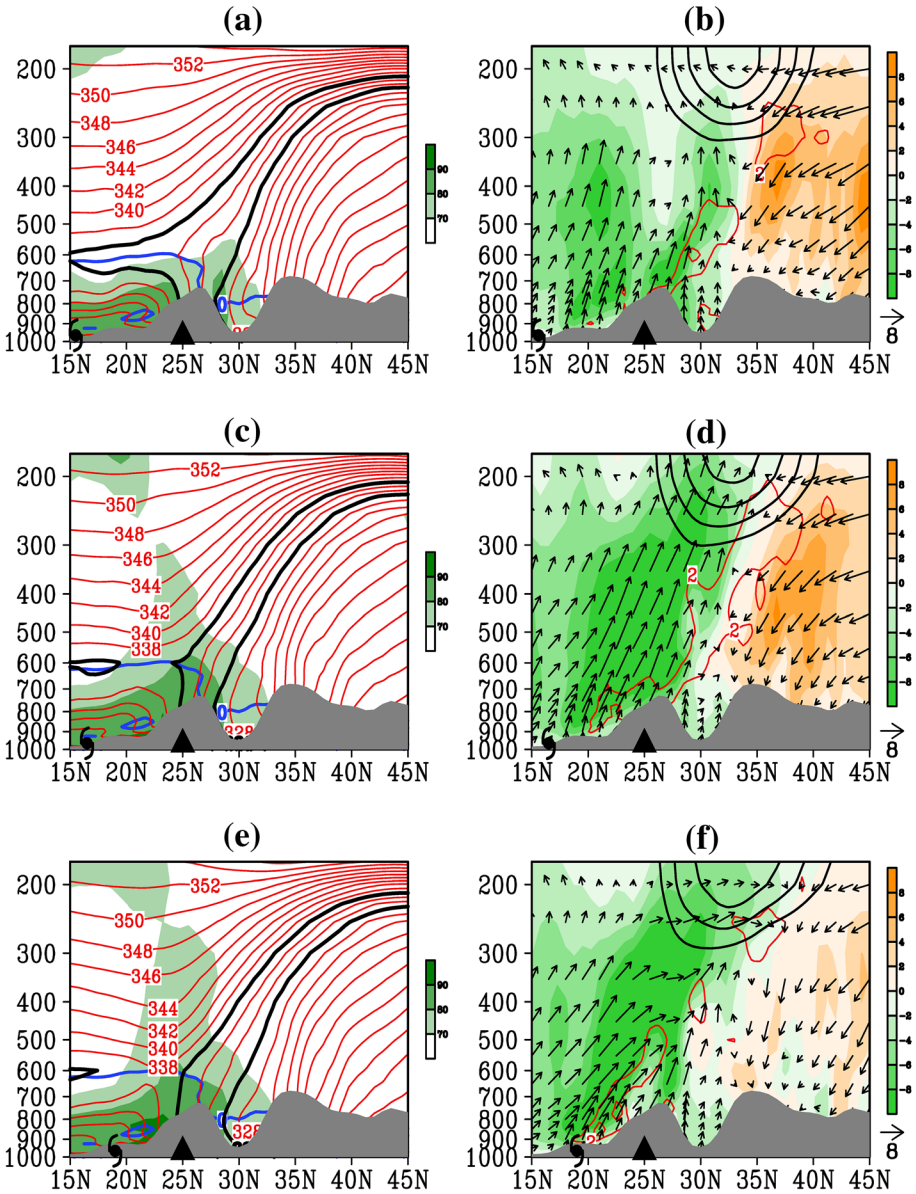

Fig. 17 Composite vertical cross-sections for 17 PRE_NE cases of relative humidity (shaded with greater than 70%), and equivalent potential temperature θ_{se} (*red contour*, unit: K; *bold black* contours mark the 330 and 336 K isolines), and the atmospheric stability (with the area of $\frac{\partial \theta_{se}}{\partial p} \geq 0$ contoured in *blue solid lines*) in left panels, and vertical velocity anomaly (*shaded*, unit: 10^{-2} pa s^{-1}), frontogenesis (*red* contours, unit: 10^{10} K m^{-1} s^{-1}), zonal wind speed (every 5 from 30 m s^{-1}, *bold black lines*), and flow in the plane of the cross-section (the *horizontal* flow is in m s^{-1}, and the *vertical* flow is in 10^{-2} pa s^{-1} in right panels for the zonal average at 97–108°E at T − 24 (**a, b**), T − 0 (**c, d**), and T + 24 (**e, f**)

15 of the total 17 PREs' initiation occur with the 200 hPa East Asia trough maintaining in the downstream of the EASJ. These results suggest that the EASJ intensification was likely influenced by both the TC-related diabatically driven outflow and maintenance of the downstream trough.

During the period of T − 0 to T + 24, the diabatically driven outflow, which originated from the TC and PRE regions to the EASJ streak, is weakened (Fig. 18d, f). The 200 hPa East Asia trough shows eastward displacement. The intensity of EASJ is also weakened, and the maximum wind speed center eastward to 125°E (Fig. 18c, e). Examination of individual cases reveals that 13 out of 17 PREs are accompanying with the eastward displacement of the EASJ from T − 0 to T + 24. The displacement of the upper-level jet may acts as an important factor in the dissipation of a PRE (Galarneau et al. 2010). Accompanying with the eastward downstream displacement of EASJ, the associated ascent forcing which is favorable for PRE occurrence over the CLLH may not exits.

6 Summary and discussion

In this paper, the remote rainfall effects of BOB TCs on CLLH were investigated from a synoptic climatological perspective. During the period of 1981 to 2012, approximately 19% of all BOB TCs produced PREs over CLLH. The PREs occur more frequently in the pre-monsoon and post-monsoon seasons with peaks in May and October, respectively. TCs formed in the pre-monsoon season are

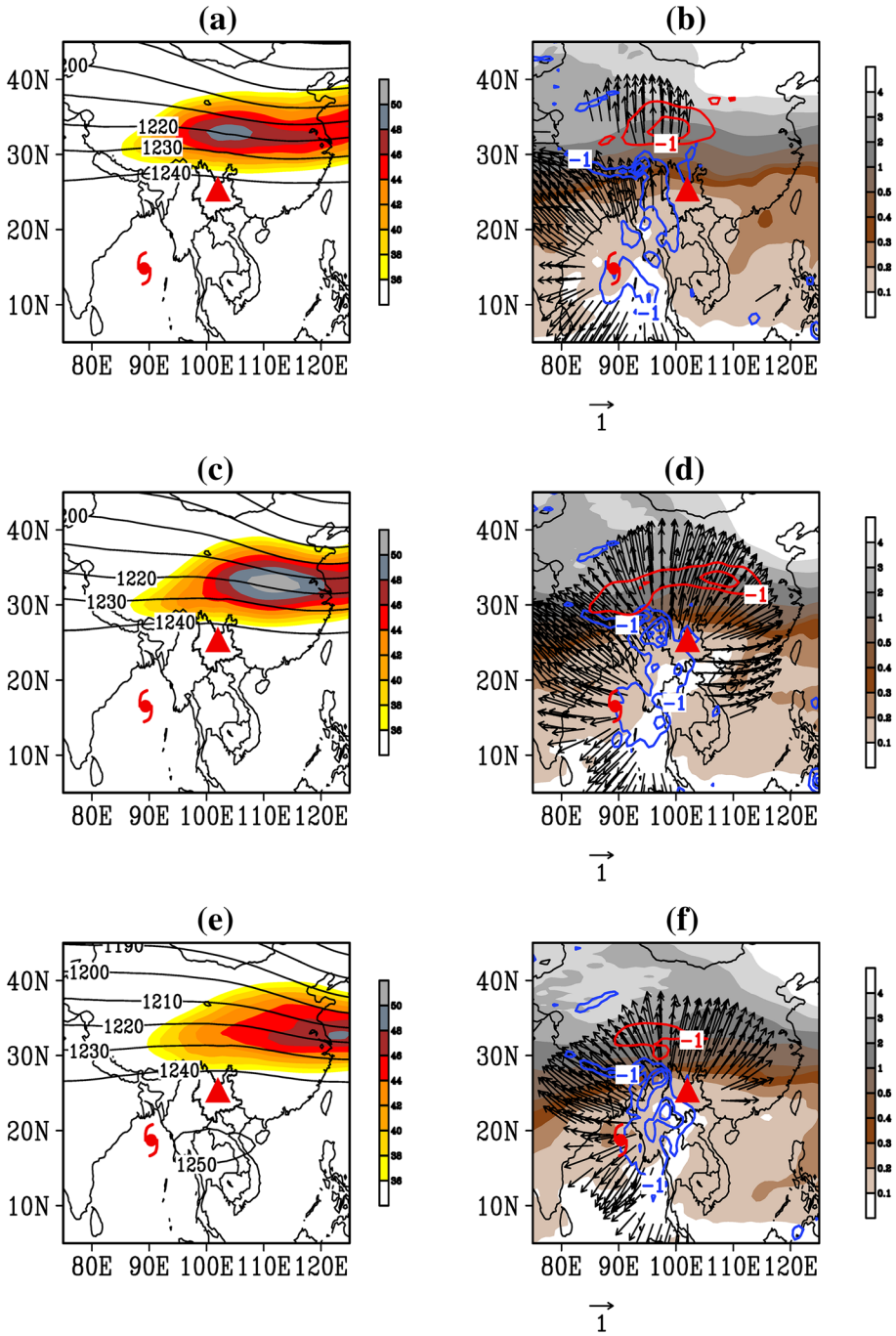

Fig. 18 Same as Fig. 13, but for 200 hPa geopotential height (*contour*, unit: *pgdm*), and zonal wind speed (*shaded*, unit: m s^{-1}) in left panels, and 250–200 hPa layer-averaged anomalous irrotational wind which is compared with the long-term climatology for 1981–2012 (plotted for irrotational wind speeds ≥1.5 m s^{-1}), PV (*shaded*, unit: 1PVU), PV advection by the anomalous irrotational wind in the 250–200 hPa layer (negative values contoured in *red* every 2 PVU day^{-1} starting at −2 PVU day^{-1}), and 700–500 hPa layer-averaged vertical velocity (contoured in *blue* every 10^{-1} pa s^{-1} starting at −1 10^{-1} pa s^{-1}) in right panels at T − 24 (**a, b**), T − 0 (**c, d**), and T + 24 (**e, f**)

more likely to produce PREs over CLLH than in the post-monsoon season. Even very weak BOB TCs may also produce PREs in CLLH. Result shows that approximately 81% of all PRE parent TCs is at or weaker than TS strength at the time of PRE initiation. The PREs occur frequently in CLLH, especially in the southwest, when TCs are active in the northern BOB and track northeastward. The median PRE lifetime is two days. BOB TCs can produce remote PREs in CLLH with the median maximum daily rainfall of 73 mm. The distances between the PREs and parent TCs vary widely from 745 to 1849 km, with a median distance of 1118 km.

The key configurations favorable for PRE occurrence over CLLH are the westward extension of the western North Pacific subtropical high dominating the South China Sea, a trough that is partially a signature of the TC circulation presented in the northern BOB, and the East Asia long-wave trough located in the east coast of China. The PRE regions are situated beneath the equatorial-ward entrance of the EASJ. The southwesterly flow appears associated

with strong pressure gradient between the subtropical high and the BOB trough, which is beneficial for steering TCs conveying abundant water vapor from the BOB to the PRE regions over CLLH. Accompanying PRE development, the robust southwesterly flow, which is present as a low-level jet in some individual cases, steers the TCs and transports moisture poleward and that convergence, frontogenesis, and ascent occur at the intersection of strong southwesterly flow with the windward side of the CLLH.

In addition, the upper-level EASJ, which is situated above and north of CLLH and located upstream of the 200-hPa East Asia trough, also plays an important role in development of PREs. The EASJ is intensified by both the upper-level trough maintained in the downstream and diabatically driven outflow related to TC, prior to the occurrence of PRE. Associated with the intensification of the EASJ, strong ascent and frontogenesis appear beneath the equatorward entrance of the EASJ, reinforcing the favorable conditions for PRE occurrence therein. Thus, for the development of the PREs in CLLH, BOB TCs seem to not only play a role in providing moisture, which is transported by the low-level southwesterly flow, but also play a dynamical role by intensifying the upper-level EASJ.

Moore et al. (2013) summarized that PREs typically occur when a low-level jet advects abundant warm moisture from the vicinity of a TC to a quasi-stationary baroclinic zone beneath the equatorial-ward entrance region of the upper-level jet streak. BOB TC-related PREs over CLLH occur with similar key configurations. Despite these common characteristics, the underlying topography over CLLH complicates the environments and likely plays an important role in PREs. The topographically influenced processes, such as orographic lifting and frontogenesis (Maddox et al. 1979; Cote 2007; Srock and Bosart 2009; Wang et al. 2009a, b), are associated with the development of PREs in CLLH, especially in the southwest. The topography distribution of CLLH is higher in the northwest with the highest altitude is over 6000 m above sea level, but lower in the southeast with the lowest altitude is below 100 m. The southwesterly flow impinges upon the mountains almost perpendicularly. The southwesterly warm and moist air flow that originated from TC vicinity can causes strong convergence, thus forces sloped ascent on the windward slope side. The moisture also extends to the mid-troposphere and thickens the saturated moist layer. The areas with conditional instability expand from the ground to 600 hPa level, which is favorable for heavy rainfall occurrence over CLLH. Case studies indicated that the slantwise ascent over the CLLH can produce heavy rainfall even in weak stable stratification conditions by evoking the conditional symmetric instability mechanism (Wang et al. 2010; Lü et al. 2013). However, there are some questions remain unclear. Does the conditional symmetric instability mechanism exits in the occurrence of PREs? How the sloping region of frontogenesis and the upper level jet are aspects of a deep jet-front system? This study show that the topography may plays an important role in PREs, but to what extent the topography contributes to the PREs? These are worthwhile to discuss in the future.

We aimed to provide climatological guidelines for forecasters to predict heavy rainfall over CLLH in relation to BOB TCs. However, this paper only shows statistical and composite results, and numerical simulations are needed, especially to quantify the effect of TC moisture and topography on TC-related PRE occurrence. However, this is challenging, as it is currently difficult to properly represent topographic and mesoscale weather system features over CLLH in numerical simulation models (Wang et al. 2011; Duan and Duan 2015).

Acknowledgements We thank Dr. Lan Xia and Dr. Tao Feng for providing helpful discussions. This work was supported by the National Natural Science Foundation of China (41305078; U1502233; 41305043), the program of KLME1304, and the Chinese Jiangsu Collaborative Innovation Center for Climate Change.

References

Bosart LF, Carr FH (1978) A case study of excessive rainfall centered around Wellsville, New York, 20–21 June 1972. Mon Wea Rev 106: 348–362

Bosart LF, Cordeira JM, Galarneau TJ, Moore BJ, Archambault HM (2012) An analysis of multiple predecessor rain events ahead of Tropical Cyclones Ike and Lowell: 10–15 September 2008. Mon Wea Rev 140: 1081–1107

Byun KY, Lee TY (2012) Remote effects of tropical cyclones on heavy rainfall over the Korean peninsula—Statistical and composite analysis. Tellus 64:14983. doi:10.3402/tellusa.v64i0.14983

Cao J, Yao P, Wang L, Liu K (2014) Summer rainfall variability in low-latitude highlands of china and subtropical indian ocean dipole. J Clim 27(2):880–892

Chen LS (2007) Study and forecast on Landfall tropical cyclone heavy rainfall. Proceeding of the 14th Proseminar on Tropical Cyclone, Shanghai, pp 3–7 **(in Chinese)**

Chen LS, Li Y, Cheng ZQ (2010) An overview of research and forecasting on rainfall associated with landfalling tropical cyclones. Adv Atmos Sci 27(5): 967–976

Chu JH, Sampson CR, Levine AS, Fukada E (2002) The Joint Typhoon Warning Center tropical cyclone best-tracks, 1945–2000. U.S. Naval Research Laboratory Rep. NRL/MR/ 7540-02-16, 22

Cong CH, Chen LS, Lei XT, Li Y (2014) A study on the tropical cyclone remote precipitation-statistical and diagnostic analyses. J Meteor Res 27. doi:10.1007/s13351-014-2070-6

Cote MR (2007) Predecessor rain events in advance of tropical cyclones. Dissertation, State University of New York

Dee DP, Uppala SM, Simmons AJ, Berrisford P, Poli P, Kobayashi S, Andrae U, Balmaseda MA, Balsamo G, Bauer P, Bechtold P, Beljaars ACM, vande Berg L, Bidlot J, Bormann N, Delsol C, Dragani R, Fuentes M, Geer AJ, Haimberger L, Healy SB, Hersbach H, Holm EV, Isaksen L, Kallberg P, Kohler M, Matricardi M, McNally AP, Monge-Sanz BM, Morcrette J-J, Park

B-K, Peubey C, de Rosnay P, Tavolato C, Thepaut J-N, Vitart F (2011) The ERA-Interim reanalysis: configuration and performance of the data assimilation system. Q J Roy Meteorol Soc 137: 553–597

Draxler RP, Hess GD (1998) An overview of the HYSPLIT_4 modeling system for trajectories, dispersion, and deposition. Aust Meteor Mag 47: 295–308

Duan X, Duan W (2015) Impact of Bay of Bengal storms on precipitation over Plateau Area. Plateau Meteorol 34(1): 1–10 **(in Chinese)**

Duan X, Tao J, Cun C, Guo S, Lü L (2009) Temporal and spatial distributions of storms over the Bay of Bengal and its activity characteristic. Plateau Meteorol 28(3): 634–641 **(in Chinese)**

Gaffney SJ (2004) Probabilistic Curve-Aligned Clustering and Prediction with Regression Mixture Models. Ph.D. thesis, Departament of Information and Computer Science. University of California, Irvine, CA

Galarneau TJ, Bosart LF, Schumacher RS (2010) Predecessor rain events ahead of tropical cyclones. Mon Wea Rev 138: 3272–3297

Huang DQ, Zhu J, Zhang YC, Huang AN (2014) The different configurations of the East Asian polar front jet and subtropical jet and the associated rainfall anomalies over eastern China in summer. J Clim 27:8205–8220. doi:10.1175/JCLI-D-14-00067.1

Kalnay E, Kanamitsu M, Kistler R et al (1996) The NCEP/NCAR 40-Year Re-analysis Project. Bull Am Meteor Soc 77: 437–472

Kistler R, Kalnay E, Collins W et al (2001) The NCEP–NCAR 50-Year Reanalysis: Monthly means CD-ROM and documentation. Bull Am Meteor Soc 82:247–267

Kummerow C, Barnes W, Kozu T et al (1998) The tropical rainfall measuring mission sensor package. J Atmos Ocean Technol 15:809–817

Li CY, Zhou W (2015) Multiscale control of summertime persistent heavy precipitation events over South China in association with synoptic, intraseasonal, and low-frequency background. Clim Dyn 45: 1043–1057

Li XZ, Zhou W (2016) Modulation of the interannual variation of the India–Burma trough on the winter moisture supply over Southwest China. Clim Dyn 46 (1): 147–158

Lü AM, Wen Y, Li (2013) Study of the impact of tropical cyclone Akash (0701) over the Bay of Bengal on a heavy rainfall event in Southwest China. Chin J Atmos Sci 37(1):160–170 (**Chinese**)

Maddox RA, Chappell CF, Hoxit LR (1979) Synoptic and meso-a scale aspects of flash flood events. Bull Am Meteor Soc 60: 115–123

Moore BJ, Bosart LF, Keyser D, Jurewicz ML (2013) Synoptic-scale environments of predecessor rain events occurring east of the rocky mountains in association with Atlantic basin tropical cyclones. Mon Wea Rev 141(3): 1022–1047

Ninomiya K (1984) Characteristics of Baiu front as a predominant subtropical front in the summer northern hemisphere. J Meteor Soc Jpn 62:880–893

Petterssen S (1936) Contribution to the theory of frontogenesis. Geofys Publ 11(6): 1–27

Pierce CH (1939) The meteorological history of the New England hurricane of Sept. 21, 1938. Mon Wea Rev 67: 237–285

Qin J, Ju JH, Xie ME (1997) The climate and weather of low-latitude highland. China Meteorological Press, Beijing **(In Chinese)**

Schumacher RS, Galarneau TJ (2012) Moisture transport into midlatitudes ahead of recurving tropical cyclones and its relevance in two predecessor rain events. Mon Wea Rev 140: 1810–1827

Schumacher RS, Galarneau TJ, Bosart LF (2011) Distant effects of a recurving tropical cyclone on rainfall in a midlatitude convective system: a high-impact predecessor rain event. Mon Wea Rev 139: 650–667

Srock AF, Bosart LF (2009) Heavy precipitation associated with southern Appalachian cold-air damming and Carolina coastal frontogenesis in advance of weak landfalling Tropical Storm Marco (1990). Mon Wea Rev 137: 2448–2470

Tao Y, Cao J, Hu J, Dai Z (2013) A cusp catastrophe model of mid–long-term landslide evolution over low latitude highlands of China. Geomorphology 187:80–85. doi:10.1016/j.geomorph.2012.12.036

Wang YQ, Wang Y, Fudeyasu H (2009a) The role of Typhoon Songda (2004) in producing distantly located heavy rainfall in Japan. Mon Wea Rev 137: 3699–3716

Wang M, Li H, Duan X (2009b) Structure analysis and numerical simulation of a landing bengal storm. Meteorol Sci Technol 37(1): 12–18 **(in Chinese)**

Wang ZQ, Zhu WJ, Duan AM (2010) A case study of snowstorm in Tibetan Plateau induced by Bay of Bengal storm: Based on the theory of slantwise vorticity development. Plateau Meteorol 29(3): 703–711 **(in Chinese)**

Wang M, Duan X, Li HH, Liu JY, Fu R (2011) A sensitivity experiment to the orographic effect on the Bengal storm of Mala during its landing. Acta Meteorologica Sinica 69(3): 486–495 (In Chinese)

Webster PJ (2008) Myanmar's deadly daffodil. Nat Geosci 1:488–490

Xiao J, Pu G, Li Y, Lü X, Wang Z (2011) Comparative analysis of cyclone Akash and Nargis. J Yunnan Univ 33(s1): 111–117 **(in Chinese)**

Xu ML, Liang HL, Duan X et al (2014) Comparative analysis of precipitation difference over yunnan influenced by Bengal Bay storm in autumn. Plateau Meteorol 33(5): 1229–1239 **(in Chinese)**

Yang ZQ, Song Y, Yang RW, Liu YP (2014) The variation and influence to droughts of different intensity precipitation days during 2009 and 2011 in low-latitude highlands. J Yunnan Univ 36(5):704–714 (**Chinese**)

Yatagai A, Arakawa O, Kamiguchi K, Kawamoto H, Nodzu MI, Hamada A (2009) A 44-year daily gridded precipitation dataset for Asia based on a dense network of rain gauges SOLA 5: 137–140. doi:10.2151/sola.2009-035

Zheng JM, Ma T, Zhang WC (2013) Climate characteristics of water vapor resource over China's low-latitude highlands. J Tropical Meteorol 29(2):291–298 (**Chinese**)